Powder Technology 305 (2017) 89–98

Contents lists available at ScienceDirect

Powder Technology

journal homepage: www.elsevier.com/locate/powtec

Capillary force and rupture of funicular liquid bridges between three spherical bodies

Ji-Peng Wang [a,*], Elena Gallo [b], Bertrand François [a], Fabio Gabrieli [b], Pierre Lambert [c]

[a] Building Architecture and Town Planning Department (BATir), Université Libre de Bruxelles, Avenue F.D. Roosevelt 50, CP 194/2, 1050 Brussels, Belgium
[b] Department of Civil, Environmental and Architectural Engineering, University of Padova, via Ognissanti 39, 35129 Padova, Italy
[c] BEAMS Department, Université Libre de Bruxelles, Avenue F.D. Roosevelt 50, CP 165/56, 1050 Brussels, Belgium

ARTICLE INFO

Article history:
Received 8 July 2016
Received in revised form 26 August 2016
Accepted 26 September 2016
Available online 28 September 2016

Keywords:
Funicular state
Liquid bridges
Capillary force
Rupture distance

ABSTRACT

Capillarity in wet granular materials induces cohesion and increases the material strength due to the attractive forces acting on capillary bridges. In the funicular state, water bridges may be not only formed between two grains but also binding three or more particles, which breaks the axial symmetry of the liquid bridge. This work presents a fundamental study on capillary forces and rupture behaviours of funicular water bridges between three spherical bodies at equilibrium (or static) configurations. Funicular water clusters are numerically solved by an energy minimization approach. Experimental comparisons are made by measuring capillary forces and these confirm the validity of the numerical solutions. Evolutions of capillary forces and rupture distances are investigated systematically by moving two spheres away from the centre. The fixed water volume condition and the constant mean curvature condition are studied respectively. Comparisons are made between the un-coalesced pendular liquid rings and the coalesced funicular bridge. For a same fixed total water volume, the capillary force is weakened by water bridge coalescence to a funicular bridge when the spheres are packed together, but the situation may vary for different contact angles and inter-particle distances. For the constant mean curvature condition, water bridge coalescence does not alter capillary force significantly when particles are packed closely, but the discrepancy is larger by increasing the gap. Funicular water bridge rupture criteria are also proposed based on the studied configurations. It is observed that in general the transmission from pendular to funicular state extends the rupture distance when it has a relatively high water volume or low air-water pressure difference.

1. Introduction

Water presence in granular materials introduces capillary force between particles by water pressure and surface tension and thus significantly increases the material cohesion which keeps the sandcastle standing [1]. With relatively low water content, isolated water bridges are formed between particles and this is referred as the pendular regime. By increasing the water content to the funicular regime, the water bridges may coalesce with each other and one liquid cluster may connect more than two grains. The capillary cohesion change in the funicular state is generally milder than the sharp increase in the pendular state [2–4]. Additionally, the capillary cohesion is usually maximised in the funicular regime [3,5,6] (Fig. 1). Further raise of water content leads the material to the capillary regime as the material is nearly saturated with only entrapped air bubbles, in this state the water surface tension effect vanishes and the sandcastle collapses.

The pressure difference between air and liquid phases is named as the Laplace pressure or suction ($S = u_a - u_w$). Suction changes with degree of saturation (S_r) and the relationship between suction and degree of saturation represents the water retention property [7,8]. Conceptually, low water content corresponds to very high suction and suction decreases rapidly with water content within the pendular regime. Suction changes gently in the funicular state and soon reduced to 0 when the material is nearly saturated (see Fig. 1). The water retention property is not unique and may have a hysteresis effect during drying and wetting cycles [7,9,10].

After the pioneer works of Haines [11] and Fisher [12], the pendular water bridge has been well understood by using two spherical particles with either controlled water volume [13–20] or constant suction [21,22]. Wet granular materials has also been investigated using the Discrete Element Method (DEM) [23] with the pendular water bridge effects [17,21,24–29]. It is aware from the literature that within the pendular state, the capillary force, which represents the magnitude of inter-particle adhesive effect, and the rupture distance, which determines the total number of interactive pairs, are the main factors for the material strengthening. The X-ray tomography technique has recently been adopted to study the funicular state liquid morphology [4,30,31]. It is observed that liquid bridge coalescence leads to more complex liquid phase morphologies such as liquid trimer, pentamer and

* Corresponding author.
E-mail address: Ji-Peng.Wang@outlook.com (J.-P. Wang).

http://dx.doi.org/10.1016/j.powtec.2016.09.060
0032-5910/

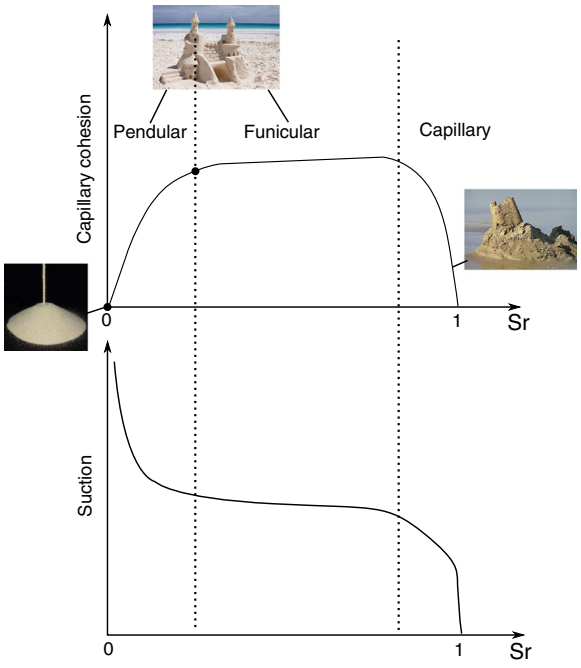

Fig. 1. Conceptual figure displaying capillary cohesion and suction in function of degree of saturation.

tetrahedron [4]. The liquid trimer, as a liquid bridge formed between three particles, is a fundamental structure of the funicular water phase presence. In this case, the study of the capillary force and rupture distance of a funicular liquid bridge between three particles could be a fundamental step toward the understanding of the capillary cohesion in the funicular state.

The two dimensional funicular water bridge effect between three discs can be analytically solved by appropriate simplifications [32,33]. It also has a very limited number of studies on the three dimensional funicular water bridge between sphere spheres [34–36]. Due to the high complexity of the geometry, analytical solutions based on Young-Laplace law are somehow sophisticated. Therefore, a numerical approach based on inter-facial energy minimization can be an alternative choice to study this problem [37]. In this work, the software tool of Surface Evolver (SE) developed by K. Brakke [38] is adopted to minimize the inter-facial energy iteratively. The funicular water bridge effect between three spherical particles is then studied systematically. The solutions are for equilibrium (or static) conditions. The evolution of capillary force and rupture criteria are investigated by lifting two spheres away from a third one steadily with a funicular water bridge formed between them. To study the macro material response under the capillary effect, water content [39–41] or suction [21,42,43] are usually controlled and varied. For this particle scale study, the water volume and suction (or Laplace pressure) are controlled respectively. An experimental test is also carried out to measure the capillary force of a funicular water bridge with various water volumes and to confirm the accuracy of the numerical solution. The effect of the contact angle and the inter-particle distance are demonstrated and rupture criteria based on the numerical solutions are proposed. The coalesced funicular water bridge effect is also compared with the un-coalesced pendular water bridges, which may qualitatively explain the capillary cohesion plateau in the funicular state.

2. Modelling and measurement of funicular water bridge

2.1. Numerical modelling

The funicular water bridge is modelled by using the Surface Evolver software. It is an iterative tool to minimize the total energy includes the surface energy and other body energies subject to various constraints. The surfaces are implemented as triangular facets. The starting liquid shapes can be defined as simplified surfaces and constraints can be applied based on liquid volume, boundary shape, mean curvature, contact angle, etc. By a gradient descent method, the software iteratively evolves the surface shape toward a condition with minimum energy. Surface mesh refinement between iteration processes can improve the solution accuracy.

The gravity effect on water bridges can be assessed by the combination of the normalised liquid volume and the Bond number, and a gravity-free domain has been discussed in [44] for the bridge between two spherical bodies. However, for the funicular water bridge, there is no clear criterion for the gravity effect. Extending the previous criterion to the funicular regime, since the radius of the spheres is relatively small ($R = 0.93$ mm) as well as the water volume used in the experiments we reasonably assumed a low gravity effect. In the following analyses, for simplicity, we will not consider the gravity effect and leave it as a future study. Therefore, without gravity, the interfacial energy will be the main energy to be minimized in the numerical solution. For a liquid bridge connecting N spheres ($N = 3$ in this study, see Fig. 2), the total interfacial energy can be calculated as:

$$E_s = \gamma A^{la} + \sum_{i=1}^{N} \gamma_i^{sl} A_i^{sl} + \sum_{i=1}^{N} \gamma_i^{sa} A_i^{sa} = \gamma A^{la} + \sum_{i=1}^{N} \left(\gamma_i^{sl} - \gamma_i^{sa}\right) A_i^{sl} + \sum_{i=1}^{N} \gamma_i^{sa} A_i \quad (1)$$

where γ is the liquid-air surface tension, A^{la} is the liquid-air interface area, γ_i^{sl} is the solid-liquid interface tension on the i-th sphere, γ_i^{sa} is the solid-air interface tension on the i-th sphere, A_i^{sl} is the solid-liquid interface area on the i-th sphere, A_i^{sa} is the solid-air interface area on the i-th sphere and A_i is the total solid surface area of the i-th sphere ($A_i = A_i^{sl} + A_i^{sa}$). The solid-air-liquid contact angle on the i-th sphere is noted as θ_i and according to the Young–Dupré equation the following relationship exists:

$$\gamma_i^{sl} - \gamma_i^{sa} = \gamma \cos\theta_i \quad (2)$$

By knowing the sphere geometry and property (sphere size and γ_i^{sa}), the term $\sum_{i=1}^{N} \gamma_i^{sa} A_i$ becomes a constant (noted as C_1). By substituting Eq. (2) into Eq. (1), the total interfacial energy is:

$$E_s = \gamma A^{la} + \gamma \sum_{i=1}^{N} \cos\theta_i A_i^{sl} + C_1 \quad (3)$$

The total interfacial energy of an initial surface shape can thus be calculated by the given surface tension γ and contact angle θ_i. Combining with an additional constraint of liquid bridge volume V, the Surface Evolver can help to minimize the total energy iteratively by a new surface shape. It should be noted that the three liquid-solid-air contact lines

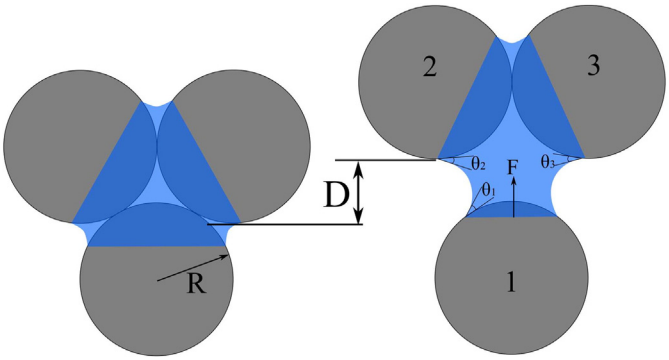

Fig. 2. Configuration of three spheres and the inter-particle distance.

are free to slip on the three spheres. Finally, the morphology of the liquid phase can be obtained after certain surface mesh refinements and iterations when the energy has little further change (less than 10^{-7} times of the total energy).

For a stable liquid bridge, the matric suction, which is defined as the pressure difference between the air and water phases, has a relationship with the mean curvature H and liquid-air surface tension γ by the Young-Laplace equation:

$$S = u_a - u_w = -2H\gamma \tag{4}$$

The pressure or the matric suction can also be maintained constantly instead of controlling the water volume V. In this case, the mean curvature of the liquid bridge will be constant and the liquid volume is varied when displacements are applied. This is the granular medium version of the nanoscale condensation problem as introduced by Chau et al. [45].

In the present study, a funicular water bridge is formed between three equally sized spherical particles. The bottom sphere is fixed and the two top particles are moved upwards (Fig. 2) until the water bridge ruptures as a case study to discuss the capillary force and rupture behaviours for both of the water volume controlled and suction controlled conditions.

The capillary force on the bottom particle can be calculated based on the virtual work principle. For a given configuration, the total energy can be obtained according to Eq. (3). We can then assume an infinitesimal displacement on the top particles asdz and recalculate the total energy for the new configuration. Then the energy difference between the two configurations is equivalent to the virtual work of the capillary force done on the displacement and we can express the capillary force as:

$$F = \frac{E_s(z+dz) - E_s(z)}{dz} \tag{5}$$

As the top two spheres are displaced away from the lower one, rupture corresponds to the distance at which convergence to a solution is not observed.

2.2. Experimental measurement

In this study, water volume controlled experimental tests are implemented to measure the funicular water bridge force as a validation of the numerical solutions. The testbed designed by Lambert [46] which is presented in Fig. 3 is employed. Three equal sized brass spheres supplied by Brammer® with $R = 0.93$ mm are used in the tests. In the setup, one sphere is glued on a cantilevered beam made of stainless steel with 0.05 mm thickness. The other two spheres are glued to a metal rod above the beam with the vertical position adjustable by a manual linear stage. The three brass spheres are cleaned by ethanol before they are glued on the beam and rod and also before each test.

In the test, a droplet of distilled water with a certain amount of volume can be generated on the bottom sphere by using a manual dispensing device and then the top rod is displaced downwards to lead the top spheres in contact with the bottom one and thus the water meniscus is formed. Then the metal rod is moved upwards gradually by the manual linear stage with a relatively low speed and the cohesive capillary force can drag the bottom sphere upwards and may cause a deflection on the cantilevered beam. The cantilevered beam, with a measured stiffness of k, acts as a spring and balances with the capillary force. The deflection of the beam (noted as δ), and the displacement of the top spheres (noted as a) are measured by two laser sensors and then the inter-particle displacement D defined in Fig. 2 can be obtained as $D = a - \delta$.

Fig. 4 represents the typical conditions of the spheres and the beam during one test. The mechanical equilibrium condition of the beam (correlated to the beam deflection δ) and the capillary force (correlated to the inter-particle distance D) are also sketched conceptually.

1) At point (1), both δ and D are equal to 0. This means that the elastic force (F_{el}) is zero and the capillary force (F_{cap}) is at the maximum without considering contact angle hysteresis. For the equilibrium of the system, this also means that the contact reaction force F_n is at the maximum.
2) The upper spheres are then pulled in vertical direction ($\delta > 0$) but D (and F_{cap}) doesn't change till the point (2) because $F_{el} < F_{cap}$. During this phase the contact force F_n decreases.
3) At the point (2) $F_{el} = F_{cap}$, while $F_n = 0$ and the bridge begins to stretch. During the stretching phase (for example point (3)), the gap increases and the beam deflection decreases.
4) At point (4), the water bridge ruptures and the beam deflection is not necessary 0.

3. Study of water volume effect

3.1. Parametric study by numerical solutions

The water volume controlled condition is firstly studied on idealised cases as a parametric study. A series of numerical solutions are obtained by assuming identical and constant contact angles on the three spheres. In Fig. 5(a), the three spheres are packed together with increasing liquid bridge volume. The relationship between the capillary force and water volume are illustrated in dimensionless terms where the force is normalised by the surface tension and particle size ($F/2\pi\gamma R$) and the liquid volume is normalised by the volume of one sphere ($V^* = V/(4/3\pi R^3)$). It can be seen that for the packed configuration, increasing volume of

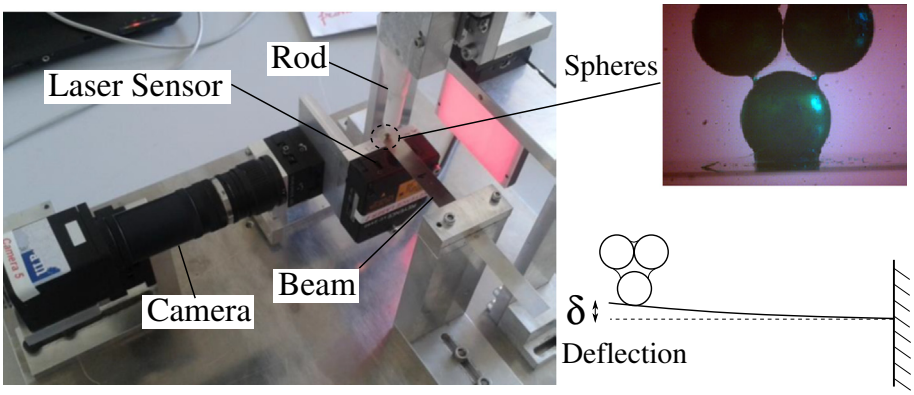

Fig. 3. The experiment device for capillary force measurement: the sphere radius is 0.93 mm and one 'bottom' sphere is glued on a steel cantilevered beam acting as a spring (stiffness noted as k) whose restoring force balances the capillary force where the deflection of the beam (δ) is measured by a laser sensor.

the funicular liquid bridge results in a lower capillary force (Fig. 5a). The effect of the contact angle is also investigated. By changing the contact angle from 0° to 60° the capillary force is reduced accordingly. This means that the capillary force is weaker on particles with a relative lower hydrophilicity (higher contact angle). It is also observed that the decreasing rate of the capillary force by contact angle is more significant for relative larger contact angles: for example the discrepancy between the results of $\theta = 0°$ and $\theta = 10°$ is negligible.

The effect of inter-particle distance (represented by the displacement D of the top spheres) is investigated by moving the top two spheres upwards at different water volumes and contact angles. In Fig. 5(b), typical results of force vs. displacement are presented for normalised water volume as 0.1, 0.2 and 0.3 with constant contact angles as 0° and 50° respectively. The curves stop at inter-particle distances for which convergence smoothness of the numerical solutions is no more reached. This distance is assumed to be the rupture distance. Increasing inter-particle distance generally reduces the capillary force, excepted for high contact angles and high water volume for which the capillary force first increases and then decreases with the inter-particle distance. The capillary force decay slope is steeper for a lower liquid volume and the rupture distance is also smaller. It is also observed that for a larger contact angle the capillary force is generally smaller at various inter-particle displacements than the results with a smaller contact angle and the contact angle effect is more significant at relative small displacements.

3.2. Experimental results and comparison

Experiments are also carried out on funicular water bridges at three different water volumes (0.3 μL, 0.6 μL and 1.2 μL) by using the testbed introduced in Section 2.2 to validate the numerical approach. Surface tension of the water used in the test is measured at room temperature as $\gamma \approx 0.073$ N/m by a pendant drop test before the capillary force measurement test. Unlike the idealised cases in Section 3.1, the contact angles are not constant in the experiment. In the capillary force measurement test, a water droplet with a certain amount of water is firstly generated on the bottom sphere and then the top rod is moved downward to be in contact with the bottom one. In this process, the solid-liquid-air contact angles on the top spheres are in advancing and as the liquid droplet is pushed down slightly by the top spheres the contact angle on the bottom sphere is also in advancing. These lead to large contact angle values on the top and bottom spheres at the very beginning of the test. Then when the top spheres are displaced upward, the liquid bridge stretches and the contact angles move progressively toward the receding contact angle. This process is not instantaneous and the contact angles evolve between advancing and receding ones during the stretching of the meniscus.

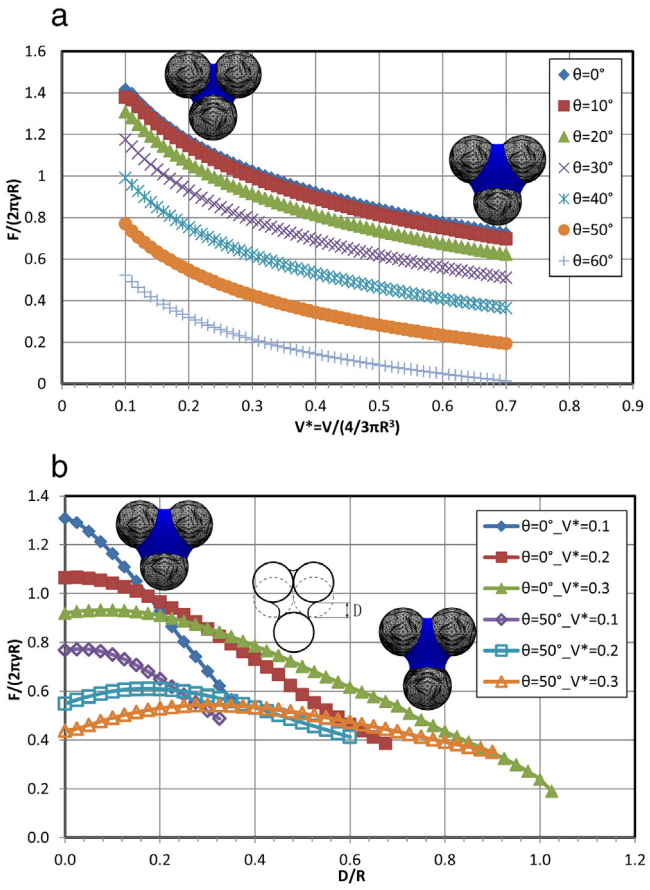

Fig. 5. Typical numerical solutions for the water volume controlled condition. (a) Force vs. water volume for spheres in contact. (b) Force vs. displacement.

Typical images for the water bridge with $V = 0.6$ μL at different displacements are presented in Fig. 6(a) in which an obvious decrease in contact angles by displacement can be observed. This phenomena is also observed by Soulié et al. in [17] for a water bridge between two spheres. The contact angle changes from advancing one to receding one can lead to a pinning effect on capillary force [47]. This means the capillary force is smaller than that of the idealised case when $D = 0$ and the force may rise and decrease to approach to the theoretical values when the contact angle decreases (Fig. 6(b)). In the laboratory experiment, the contact angles are measured by image analysis. It is observed that the contact angles on the top spheres are generally larger than that on the bottom sphere. Fig. 7(a) and Fig. 7(b) present the

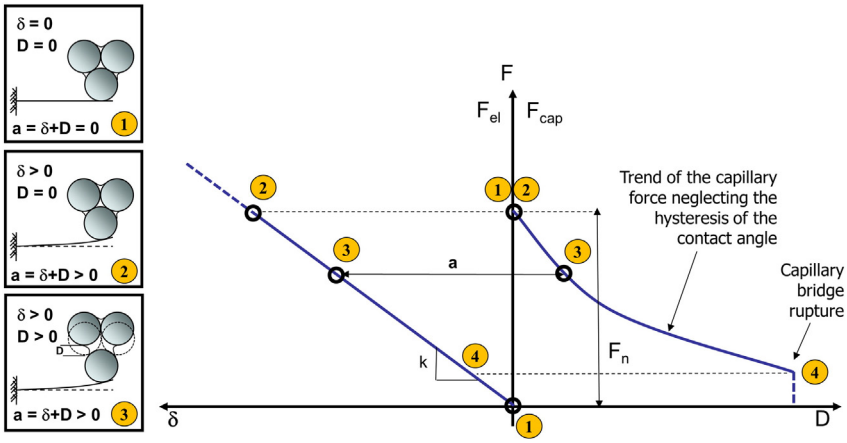

Fig. 4. Different conditions of beam deflections and capillary force measurements.

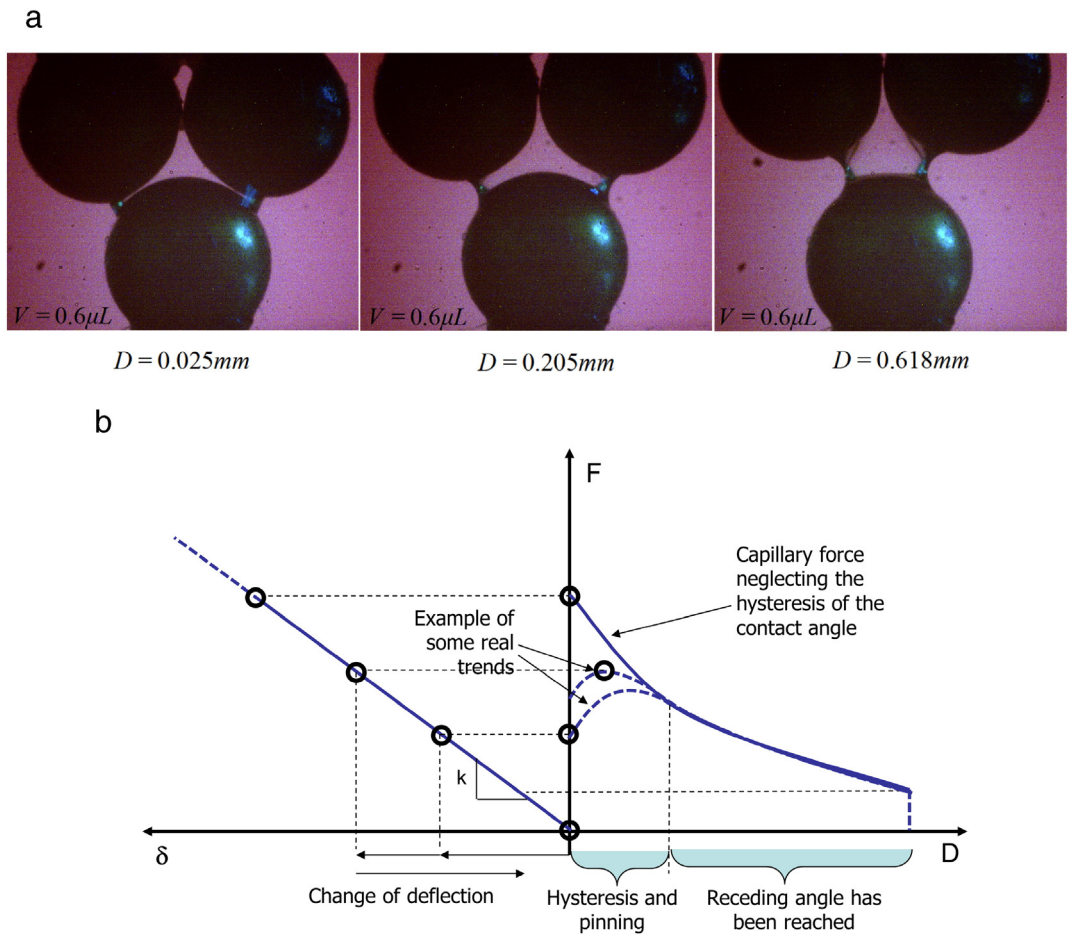

Fig. 6. Effects of contact angle hysteresis and pinning. (a) Conceptual sketch of the real measurement. (b) Water bridge images at different displacements.

measured upper and lower contact angles in scatters by taking an average on the left and right side values. 3rd order polynomial fits are also illustrated in solid or dash lines.

The measured contact angles at different displacements are then be input into Surface Evolver to reproduce the laboratory experiment. We use the polynomial fitting equations as the input parameters to assign contact angles in the numerical simulations. The experimental results (scatters) and the numerical solutions (lines) are depicted in Fig. 8 in normalised forms for comparison. Due to the pinning effect [47], an increase in capillary force with increasing separation distance is observed and after the contact angle reduced to the receding angles the three phase contact line on the bottom sphere stat to slip and leads to a decrease in capillary force until rupture. The numerical solutions (plotted as lines) generally have a fair agreement with the experiment results and only some shifts are observed in the positions of the maximum forces. The discrepancies between the experimental measurements and numerical solutions in Fig. 8 may be induced by the roughness of the spheres, errors in contact angle measurement and the asymmetry of the liquid phase. Nevertheless, it can be seen that the numerical approach achieved reasonable solutions on this problem and thus it can be employed for further discussions like water bridge coalescence and rupture distance in the following sections.

3.3. Effect of water bridge coalescence

In the pendular state, water bridges are formed between particle pairs and capillary force has a clear analytical solution which is widely adopted in DEM simulations [48–51]. By increasing water content, the assumption of the pendular water bridge in DEM simulation is no longer valid as they may overlap with each other and in reality they will coalesce and form a funicular water bridge. The effect of water bridge coalescence therefore should be investigated.

Two scenarios are compared in this study (Fig. 9). In the first scenario the funicular water bridge with a particular water volume is formed between particles and the capillary effect is numerically solved for different displacement. Another scenario is that the same amount of water is split into three pendular water bridges connecting the three particles. The volumes of the pendular water bridges are assumed to be identical ($3V_1 = V$) and the possible water bridge overlapping is ignored. The capillary force on the bottom sphere is then calculated from the force projection on the vertical direction based on the analytical solution of a pendular water bridge [17] in which the capillary force on a pendular water bridge is expressed as:

$$F_1 = \pi\gamma R\left[\exp\left(a\frac{D_1}{R}+b\right)+c\right] \tag{6}$$

where $a = -1.1\left(\frac{V_1}{R^3}\right)^{-0.53}$, $b = (-0.148\ln\left(\frac{V_1}{R^3}\right)-0.96)\theta^2-0.0082\ln\left(\frac{V_1}{R^3}\right)+0.48$, $c = 0.0018\ln\left(\frac{V_1}{R^3}\right)+0.078$ and $D_1 = \sqrt{R^2+(\sqrt{3}R+D)^2}-2R$ in which $V_1 = \frac{V}{3}$ is the liquid volume in one pendular bridge, R is the particle radius, θ is the contact angle and D_1 is the inter-particle distance between two particles. By projecting the forces, the vertical force on the bottom sphere is:

$$F = \frac{2\left(\sqrt{3}R+D\right)F_1}{\sqrt{R^2+\left(\sqrt{3}R+D\right)^2}} \tag{7}$$

where D is the vertical displacement of the top spheres.

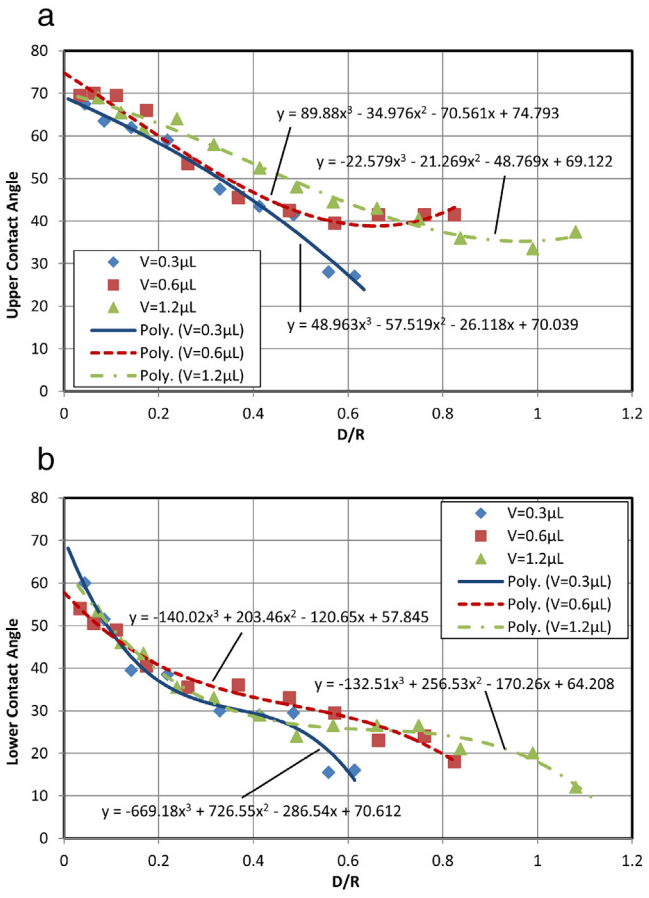

Fig. 7. Measured contact angle values: (a) contact angle on upper spheres, (b) contact angle on the lower sphere.

As the pendular water bridge solutions are based on idealised cases, we still take the condition that the contact angle on each sphere is identical and constant to discuss the water bridge coalescence effect. In Fig. 10, the numerical simulation results from Fig. 5(b) and the estimation from the pendular water bridges from Eqs. (6) and (7) are compared at different total liquid volumes (normalised total liquid volume as $V^* = 0.1$, 0.2 and 0.3) and contact angles ($\theta = 0°$ and 50°) in normalised forms. When the spherical particles are closed with each other, the capillary force on the funicular water bridge is smaller than the un-coalesced water bridges. By lifting the top spheres upwards, the discrepancies between numerical solutions on the funicular water

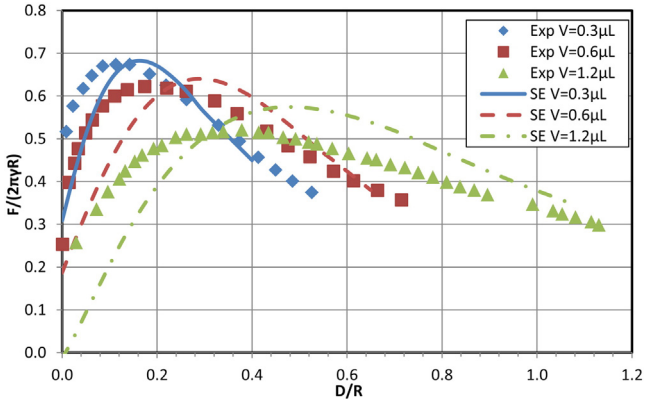

Fig. 8. Comparison between the numerical solutions (curves) and experiment results (points).

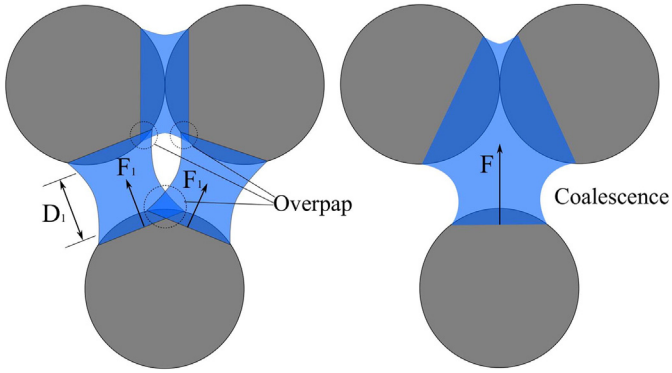

Fig. 9. Water bridge overlap and coalescence.

bridge and estimations based on un-coalesced water bridges become smaller, especially for a lower contact angle.

3.4. Rupture criteria

By Lian et al. [15], the rupture distance of a pendular water bridge is a function of liquid volume and contact angle as:

$$D_{pen}^{rupture} = (1 + 0.5\theta)V_1^{1/3} \tag{8}$$

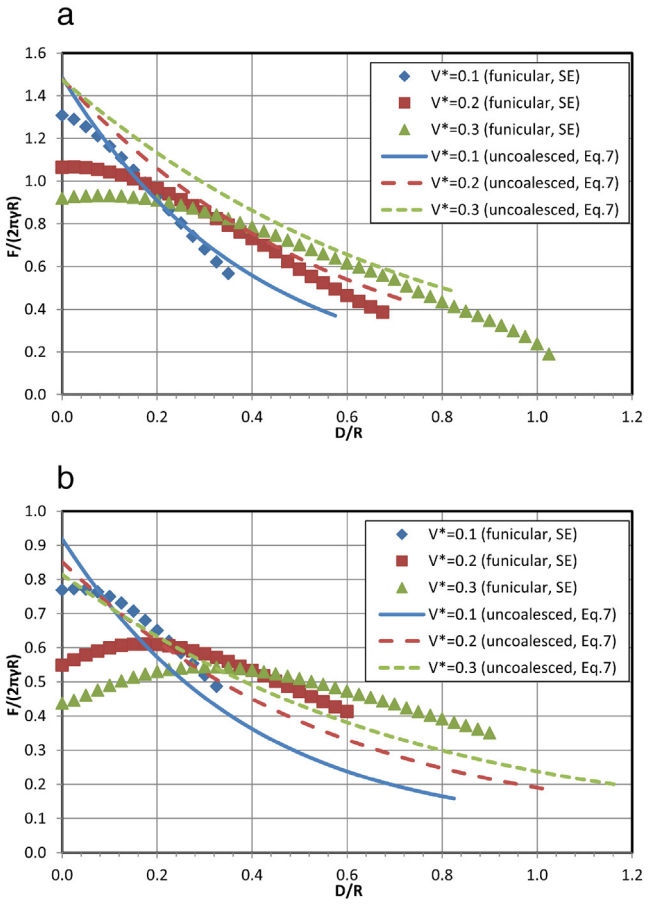

Fig. 10. Effect of water bridge coalescence under water volume controlled condition: the points are the funicular water bridge results and the curves are estimations from the uncoalesced pendular water bridges by Eq. (7). (a) Contact angle $\theta = 0°$. (b) Contact angle $\theta = 50°$.

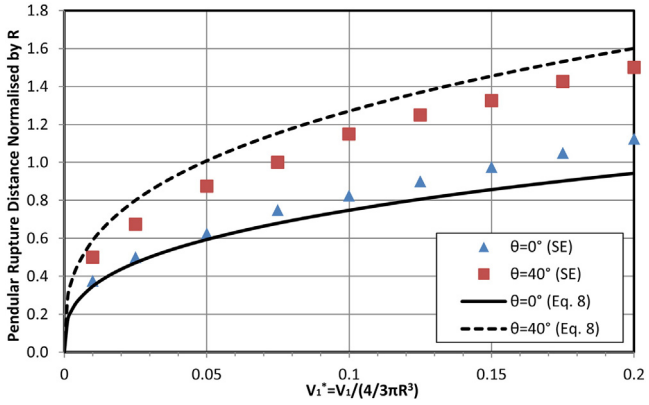

Fig. 11. Rupture distance of the volume controlled pendular liquid bridge.

where V_1 represents the water volume on one water bridge and θ is the contact angle. In this study, water bridge rupture is assumed to happen at the point where there are no more convergence nor smooth solutions. A validation has been carried out on the pendular regime based on the numerical solved rupture distance. A series of pendular water bridge are numerical simulated with various volumes at two constant contact angles (0°and 40°) and the numerical solutions are compared with the prediction by Eq. (8) in Fig. 11. The water volume is normalised as $V_1^* = V_1/({}^4/_3\pi R^3)$ and the distance is normalised by the particle radius. It can be seen that the numerical solutions agree well with the predictions by Lian's criteria and we can extend the rupture behaviour study to the funicular bridges.

More numerical solutions are then implemented in funicular regime with various liquid volumes and contact angles and the rupture distance, at where there is no more convergence nor smooth solutions, are analysed. In Fig. 12, the rupture distance is plotted against the liquid volume in dimensionless terms where the rupture distance is normalised by particle size and the liquid volume is normalised by the volume of one sphere ($D^*_{rupture} = \frac{D_{rupture}}{R}$ and $V^* = V/({}^4/_3\pi R^3)$). It is observed that when the liquid volume is smaller than a certain value (V^*<0.06), the water bridge connecting three particles cannot be formed which means the spheres can only be bonded by pendular rings. Beyond this value, funicular water bridge can be generated and the rupture distance ascends with the water volume. The rupture distance of a funicular water bridge is not obviously affected by contact angle in the studied range (θ<40^0). The following equation can be adopted to fit the rupture distance of a funicular water bridge in the configuration studied:

$$D^*_{rupture} = \frac{D_{rupture}}{R} = 2.6(V^* - 0.06)^{2/3} \tag{9}$$

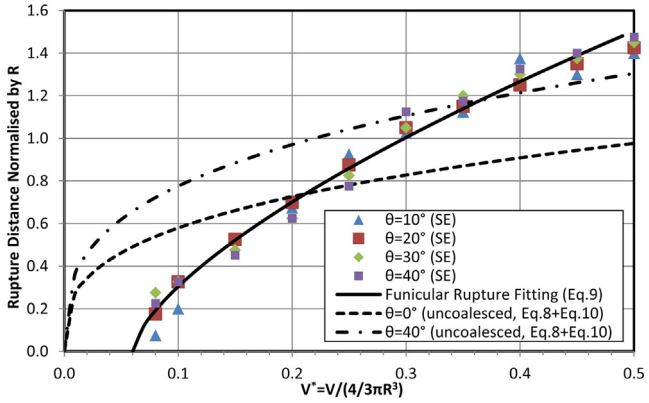

Fig. 12. Rupture distance for the volume controlled funicular water bridge.

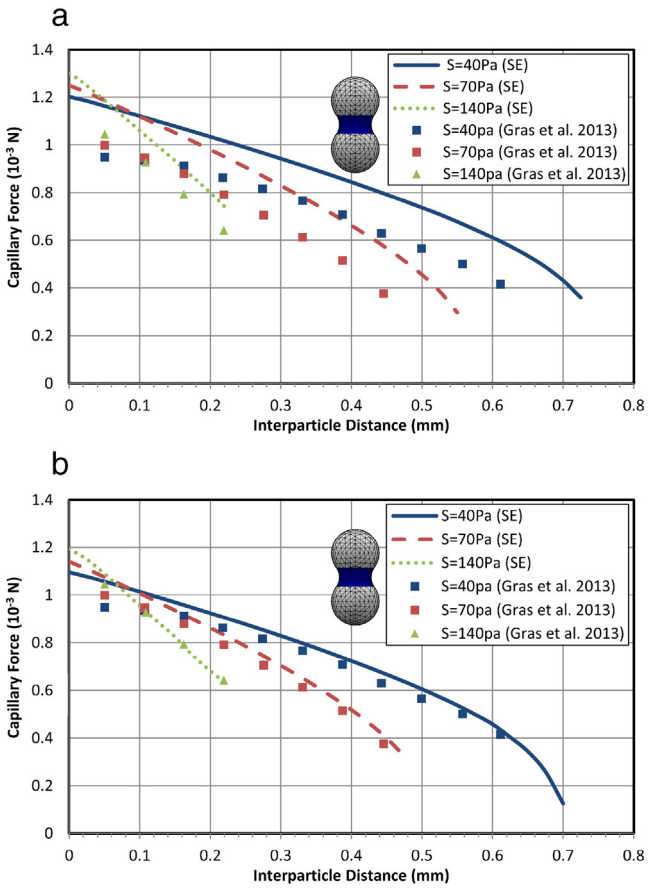

Fig. 13. Verification for the suction controlled test (experimental results are given by Gras et al. [22]). (a) Comparison with numerical solution as $\theta = 20°$. (b) Comparison with numerical solution as $\theta = 30°$.

For the configuration of the un-coalesced case in Fig. 9, the maximum vertical displacement of the top spheres before rupture can be estimated as from the geometrical relationship:

$$D_{est}^{rupture} = \sqrt{\left(2R + D_{pen}^{rupture}\right)^2 - R^2} - \sqrt{3}R \tag{10}$$

By substituting Eq. (8) into Eq. (10), the estimated rupture distances from the pendular water bridges are obtained and thus also presented in Fig. 12 as a normalised form ($D_{est}^{rupture}/R$) which are referred as the 'uncoalesced' condition. The possible water bridge overlap is ignored in the estimations and the estimations are made at two contact angles (0°and 40°). It can be seen that the water bridge coalescence shortens the rupture distance when the water volume is relatively small but however extends the rupture distance when the liquid volume is higher. The water bridge coalescence also reduces the effect of contact angle as the contact angle effect is considerable in the pendular state liquid bonds but negligible in the funicular state.

4. Study of suction effect

4.1. Verification of an experiment test on two spheres

Besides controlling water volume, a suction controlled condition, which means the mean curvature of the liquid bridge is constant, is also investigated. Typical solutions can be obtained at various configurations by using the numerical modelling with Surface Evolver. The suction controlled test is not able to be reproduced by the test in Fig. 3. However, Gras et al. developed a device to measure the capillary force of a pendular water bridge formed between two spheres with the

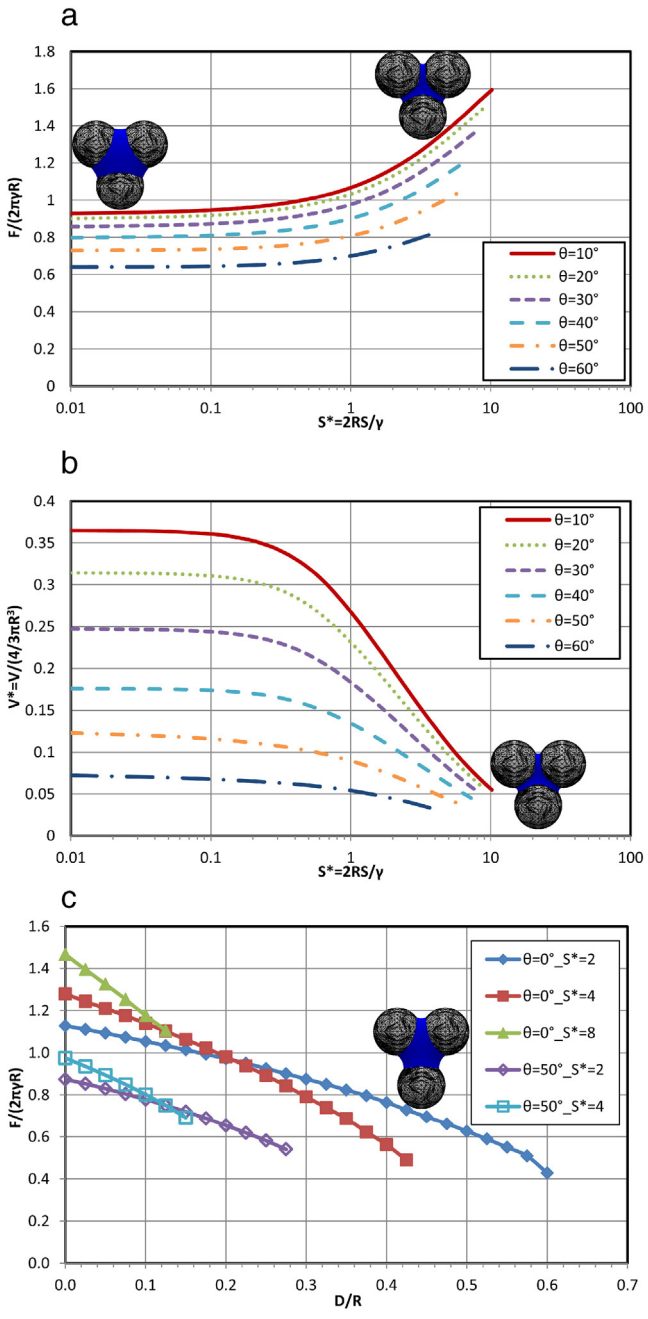

Fig. 14. Typical numerical solutions for the suction controlled condition. (a) Force vs. suction for spheres in contact ($D = 0$). (b) Water volume vs. suction for spheres in contact ($D = 0$). (c) Force vs. displacement.

suction being controlled [22]. In the test, the radius of the two spheres is about 5 mm. Three suction values are controlled as 40 Pa, 70 Pa and 140 Pa respectively. The liquid-solid-air contact angle is measured as 20° by image analysis by the authors of the experiments and the liquid surface tension is claimed to be 0.051 N/m. The suction controlled pendular state water bridge is reproduced by the numerical tool by using the same parameters and the solved capillary force is compared with this experimental data in Fig. 13(a). It can be seen that the numerical solution only has a slight overestimation comparing to the experimental results and the general trend is in consistency. However, as errors may exist during the contact angle measurement from images, we also solved the same liquid bridges by using a different contact angle ($\theta = 30°$) in Fig. 13(b) in which numerical solutions are quite closed to the experimental data. After the two comparisons, the numerical tool can be considered to be a trustable approach for the suction controlled conditions.

4.2. Numerical solutions of the funicular water bridge

After this validation in pendular state with two spheres, the numerical solution is extended to funicular state as a water bridge being formed between three spheres. Firstly, the capillary force of the funicular water bridge is studied for three spheres in contact with each other in Fig. 14(a) in which suction is expressed as a dimensionless term of $S^* = 2RS/\gamma$ and S^* is in logarithm scale. A raise of suction, which means a decrease of water volume correspondingly, leads to a higher capillary force. The contact angle effect is also significant for the suction controlled condition as larger contact angle reduces the capillary force. The relationship between the normalised water volume and the normalised suction is presented in Fig. 14(b). For a same suction value, a lower contact angle leads to a higher water volume. This means the change of contact angle during the wetting and drying process of a wet granular material is one of the reasons of the hysteresis effect of water retention curve. As the water content of a granular material is being dried is generally higher than that of the material is being wetted at the same suction level.

Then a same particle displacement is applied while the suction is controlled as a constant in which the top two spheres are lifted up and the capillary force on the bottom sphere is calculated by Eq. (5). Fig. 14(c) depicts the relationship between the displacement and the capillary force at different contact angles and suctions. Capillary force is reduced by lifting the spheres up and the rupture distance is shorter for higher suction level. By increasing the contact angle, not only the capillary force becomes weaker, the rupture distance is also shortened. For $S^* = 8$, when $\theta = 0°$ there is a numerical solution, but when the contact angle is increased to 50° there is no more convergence of the numerical solutions. Just like the water volume controlled condition, the effect of water bridge coalescence on force and rupture distance is worth to be discussed.

4.3. Effect of liquid bridge coalescence

Similar to the water volume controlled condition; the difference between the un-coalesced and coalesced water bridges under constant suctions are investigated. In Fig. 15, the numerical results of the suction controlled funicular water bridge are plotted in scatters in comparison with the approximated results of the pendular bridges without considering the water bridge overlap (plotted in lines). The funicular water bridge is evolved at three different normalised suction values and the contact angle is 0°. The capillary forces of pendular water bridge are also solved by the numerical tool at the same suction level and contact angle and then converted to the vertical force on the bottom sphere by Eq. (7). It can be seen that when the spheres are packed together, the funicular water bridge induced capillary forces are closed to the pendular water bridge approximations especially for a low suction value. However, by lifting the top spheres away, the discrepancies

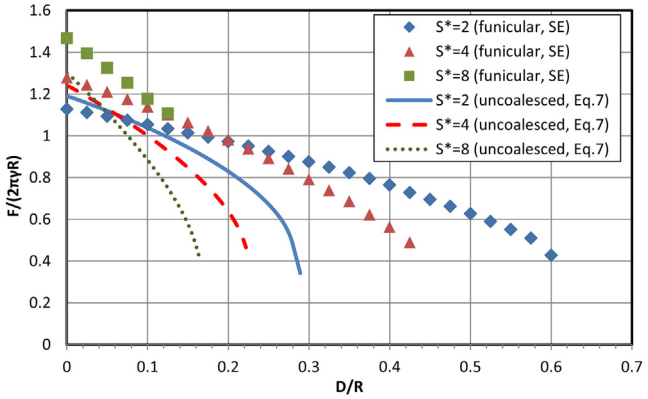

Fig. 15. Effect of water bridge coalescence under suction controlled condition ($\theta = 0°$).

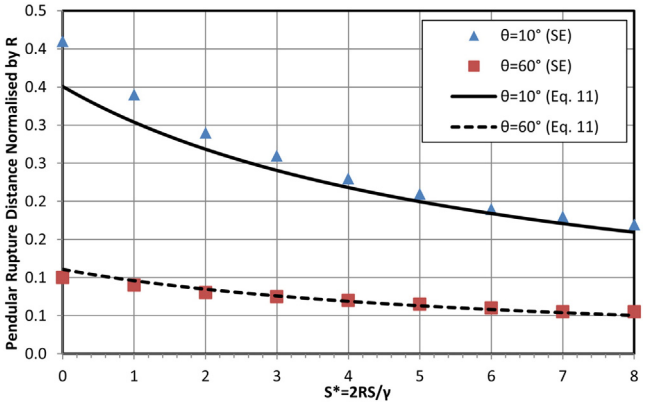

Fig. 16. Rupture distance of suction controlled pendular water bridge.

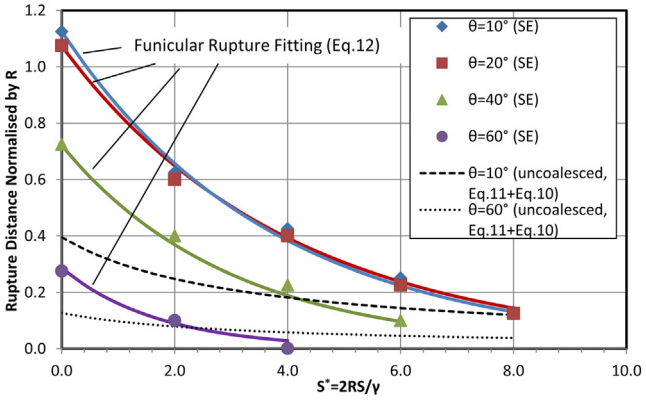

Fig. 17. Rupture distance for the suction controlled funicular water bridge.

between the funicular water bridge solutions and the pendular approximations develop rapidly and it can be seen that the rupture distance of the funicular water bridge is much larger. This means under constant suction condition, the water bridge coalescence in the transmission from the pendular state to the funicular state may significantly extend the rupture distance. Although when spheres are packed together the water bridge coalescence doesn't change the capillary force much, one can expect stronger attractive force for a funicular water bridge than that of the uncoalesced bridges when there is some gap in between the particles.

4.4. Rupture criteria

The rupture criterion for a suction controlled pendular liquid bridge formed between two spheres is proposed by Gras et al. [22] empirically and the normalised form is expressed as:

$$D_{pen}^{rupture*} = \frac{D_{pen}^{rupture}}{R} = (\cos\theta)^{1.7}(0.5S^* + 3)^{-0.93} \tag{11}$$

This expression fits well with the Young-Laplace solutions with controlled suctions as claimed by the authors. By assuming the rupture distance is at the distance from where there is no more converged and smooth solutions, the pendular water bridge rupture distance between two particles are numerically solved by Surface Evolver at different suctions and contact angles. The typical results are presented in Fig. 16 in comparison with Gras's rupture criteria. It is observed that the funicular regime numerical solutions are fitted well with Gras's rupture criteria. From this basis, we can assume that the numerical solved rupture distance is also reliable in the funicular regime and extend the rupture distance study to the three spheres case.

A series of funicular water bridges between three spheres are also solved for the configuration that the bottom sphere is fixed while the top two are lifted up with various suctions and contact angles. The rupture distances are then be analysed. Fig. 17 presents the normalised rupture distance of the funicular water bridge in symbols at various contact angles and suctions. It can be seen that the increase of contact angle and suction reduced the rupture distance. We can also fit the rupture distance by an empirical equation. Firstly, the rupture distance for the condition of $S^* = 0$ is fitted as $D_{rupture}^* = 1.125(\cos(\theta - \frac{\pi}{18}))^{3.1}$ which is only related to the contact angle. Then the rupture distance is in decay with the suction and can be approximated as an exponential equation. The full form of the rupture criteria is expressed as:

$$D_{rupture}^* = 1.125\left(\cos\left(\theta - \frac{\pi}{18}\right)\right)^{3.1}\exp(kS^*) \tag{12}$$

where the parameter k determining the slope of the exponential decay is a function of the contact angle as $k = -0.6531\theta^2 + 0.4444\theta - 0.3266$. The fitted rupture distance is depicted in solid lines in Fig. 17 and agrees well with the data. By substituting Eq. (11) into Eq. (10), the rupture distance approximated by the pendular water bridges for the three spheres configuration can be obtained. The approximated results are illustrated in dash lines for two different contact angles. It can also be seen that in most cases the funicular water bridge has longer rupture distances than that of the pendular water bridges under the suction controlled condition.

5. Conclusions

In this work, a most fundamental funicular liquid bridge formed between three spheres is numerically solved by using an energy minimization technique (through Surface Evolver software). Both the volume controlled and the suction controlled conditions are explored.

For the water volume controlled condition, numerical solutions and experimental measurements have been carried out on the capillary force between three spheres. The water bridge coalescence effect is discussed based on an equivalent configuration. The following conclusions are obtained.

- The experiment results agree well with the numerical solutions and this proves the reliability of the numerical approach.
- The water bridge coalescence process has significant effect on both capillary force and rupture distance.
- For a relatively low water volume, the water bridge coalescence does not obviously change the capillary force but reduced the rupture distance.
- When the water volume is relatively large, the funicular water bridge has a lower capillary force than that of the pendular water bridges with the same total volume but the rupture distance will also be extended.
- The contact angle effect on rupture distance in the funicular state is reduced than that in the pendular state.

For the suction controlled condition:

- The contact angle in the funicular state is also an important factor for the granular material water retention behaviour hysteresis.
- Under the same suction, increase the contact angle will both decrease the capillary force and the rupture distance.
- A rupture criterion for the symmetric funicular water bridge is proposed by fitting the numerical solutions.
- Liquid bridge coalescence process which leads the transition to the funicular regime does not change the capillary force significantly when the spheres are packed together but considerably increases the rupture distance in most cases.

The cohesion of the wet granular materials is originated from the capillary force (which determines the magnitude of the inter-particle attractive effect) and the liquid bridge rupture distance (which influences the total number of the interactive particles). From this fundamental study,

we qualitatively observe that the capillary force change and the rupture distance variation by liquid bridge coalescence are not always in concert with each other. The combination effect could be the main reason of the mild cohesion change in the funicular state. However, the liquid morphology in a wet granular material is more sophisticated, for example the positions of the three particles may be more random and the liquid cluster may connect more particles. More future work is still desired on funicular liquid clusters by considering influences from contact angle, relative positions of particles, number of particles, particle roughness, particle shape, etc.

Acknowledgement

The authors wish to acknowledge the grant from FNRS (Project PDR.T.1002.14 “Capillarity in granular materials”). This work has also been supported by the IAP 7/38 MicroMAST funded by BELSPO.

References

[1] D. Hornbaker, R. Albert, I. Albert, A.L. Barabasi, P. Schiffer, What keeps sandcastles standing? Nature 387 (1997) 765-765, http://dx.doi.org/10.1038/42831.
[2] H. Schubert, Tensile strength of agglomerates, Powder Technol. 11 (1975) 107–119, http://dx.doi.org/10.1016/0032-5910(75)80036-2.
[3] N. Lu, T.-H. Kim, S. Sture, W.J. Likos, Tensile strength of unsaturated sand, J. Eng. Mech. 135 (2009) 1410–1419, http://dx.doi.org/10.1061/(ASCE)EM.1943-7889.0000054.
[4] M. Scheel, R. Seemann, M. Brinkmann, M. Di Michiel, A. Sheppard, B. Breidenbach, S. Herminghaus, Morphological clues to wet granular pile stability, Nat. Mater. 7 (2008) 189–193, http://dx.doi.org/10.1038/nmat2117.
[5] H. Schubert, Capillary forces - modeling and application in particulate technology, Powder Technol. 37 (1984) 105–116, http://dx.doi.org/10.1016/0032-5910(84)80010-8.
[6] N. Lu, J.W. Godt, D.T. Wu, A closed-form equation for effective stress in unsaturated soil, Water Resour. Res. 46 (2010), W05515 http://dx.doi.org/10.1029/2009WR008646.
[7] M.T. van Genuchten, A closed-form equation for predicting the hydraulic conductivity of unsaturated soils, Soil Sci. Soc. Am. J. 44 (1980) 892–898.
[8] D.G. Fredlund, A. Xing, Equations for the soil-water characteristic curve, Can. Geotech. J. 31 (1994) 521–532, http://dx.doi.org/10.1139/t94-061.
[9] D.G. Fredlund, A. Xing, M.D. Fredlund, S.L. Barbour, The relationship of the unsaturated soil shear to the soil-water characteristic curve, Can. Geotech. J. 33 (1996) 440–448, http://dx.doi.org/10.1139/t96-065.
[10] S.J. Wheeler, R.S. Sharma, M.S.R. Buisson, Coupling of hydraulic hysteresis and stress–strain behaviour in unsaturated soils, Géotechnique 53 (2003) 41–54.
[11] W.B. Haines, Studies in the physical properties of soils: II. A note on the cohesion developed by capillary forces in an ideal soil, J. Agric. Sci. 15 (1925) 529–535, http://dx.doi.org/10.1017/S0021859600082460.
[12] R.A. Fisher, On the capillary forces in an ideal soil; correction of formulae given by W. B. Haines, J. Agric. Sci. 16 (1926) 492–505.
[13] G. Mason, W.C. Clark, Liquid bridges between spheres, Chem. Eng. Sci. 20 (1965) 859–866, http://dx.doi.org/10.1016/0009-2509(65)80082-3.
[14] K. Hotta, K. Takeda, K. Iinoya, The capillary binding force of a liquid bridge, Powder Technol. 10 (1974) 231–242.
[15] G. Lian, C. Thornton, M. Adams, A theoretical study of the liquid bridge forces between two rigid spherical bodies, J. Colloid Interface Sci. 161 (1993) 138–147.
[16] C.D. Willett, M.J. Adams, S.A. Johnson, J.P.K. Seville, Capillary bridges between two spherical bodies, Langmuir 16 (2000) 9396–9405, http://dx.doi.org/10.1021/la000657y.
[17] F. Soulié, F. Cherblanc, M.S. El Youssoufi, C. Saix, Influence of liquid bridges on the mechanical behaviour of polydisperse granular materials, Int. J. Numer. Anal. Methods Geomech. 30 (2006) 213–228, http://dx.doi.org/10.1002/nag.476.
[18] P. Lambert, A. Chau, A. Delchambre, S. Régnier, Comparison between two capillary forces models, Langmuir 24 (2008) 3157–3163, http://dx.doi.org/10.1021/la7036444.
[19] Y.I. Rabinovich, M.S. Esayanur, B.M. Moudgil, Capillary forces between two spheres with a fixed volume liquid bridge: theory and experiment, Langmuir 21 (2005) 10992–10997, http://dx.doi.org/10.1021/la0517639.
[20] O. Harireche, A. Faramarzi, A.M. Alani, A toroidal approximation of capillary forces in polydisperse granular assemblies, Granul. Matter 15 (2013) 573–581, http://dx.doi.org/10.1007/s10035-013-0425-9.
[21] L. Scholtès, P. Hicher, F. Nicot, B. Chareyre, F. Darve, On the capillary stress tensor in wet granular materials, Int. J. Numer. Anal. Methods Geomech. 33 (2009) 1289–1313, http://dx.doi.org/10.1002/nag.767.
[22] J.-P. Gras, J.-Y. Delenne, M.S. El Youssoufi, Study of capillary interaction between two grains: a new experimental device with suction control, Granul. Matter 15 (2013) 49–56, http://dx.doi.org/10.1007/s10035-012-0388-2.
[23] P.A. Cundall, O.D.L. Strack, A discrete numerical model for granular assemblies, Géotechnique 29 (1979) 47–65, http://dx.doi.org/10.1680/geot.1979.29.1.47.
[24] V. Richefeu, M. El Youssoufi, F. Radjaï, Shear strength properties of wet granular materials, Phys. Rev. E 73 (2006) 051304, http://dx.doi.org/10.1103/PhysRevE.73.051304.
[25] V. Richefeu, M.S. El Youssoufi, E. Azéma, F. Radjaï, Force transmission in dry and wet granular media, Powder Technol. 190 (2009) 258–263, http://dx.doi.org/10.1016/j.powtec.2008.04.069.
[26] J.-P. Gras, J.-Y. Delenne, F. Soulié, M.S. El Youssoufi, DEM and experimental analysis of the water retention curve in polydisperse granular media, Powder Technol. 208 (2011) 296–300, http://dx.doi.org/10.1016/j.powtec.2010.08.019.
[27] F. Gabrieli, P. Lambert, S. Cola, F. Calvetti, Micromechanical modelling of erosion due to evaporation in a partially wet granular slope, Int. J. Numer. Anal. Methods Geomech. 36 (2012) 918–943, http://dx.doi.org/10.1002/nag.1038.
[28] J.P. Wang, X. Li, H.S. Yu, A micromechanical interpretation of the capillary effect of unsaturated granular material in a pendular state, Comput. Methods Recent Adv. Geomech. - Proc. 14th Int. Conf. Int. Assoc. Comput. Methods Recent Adv. Geomech. IACMAG 2014, Taylor and Francis, Balkema 2015, pp. 1563–1568.
[29] J.-P. Wang, X. Li, H.-S. Yu, On the stress-force-fabric relationship for unsaturated granular materials in pendular states, J. Eng. Mech. (2016) (submitted).
[30] K. Manahiloh, B. Muhunthan, Characterizing liquid phase fabric of unsaturated specimens from X-ray computed tomography images, in: C. Mancuso, C. Jommi, F. D'Onza (Eds.), Unsaturated Soils Res. Appl. Springer, Berlin Heidelberg 2012, pp. 71–80.
[31] K.N. Manahiloh, B. Muhunthan, W.J. Likos, Microstructure-based effective stress formulation for unsaturated granular soils, Int. J. Geomech. D4016006 (2016) http://dx.doi.org/10.1061/(ASCE)GM.1943-5622.0000617.
[32] M. Urso, C. Lawrence, M. Adams, Pendular, funicular, and capillary bridges: results for two dimensions, J. Colloid Interface Sci. 220 (1999) 42–56, http://dx.doi.org/10.1006/jcis.1999.6512.
[33] M.E.D. Urso, C.J. Lawrence, M.J. Adams, A two-dimensional study of the rupture of funicular liquid bridges, Chem. Eng. Sci. 57 (2002) 677–692, http://dx.doi.org/10.1016/S0009-2509(01)00418-3.
[34] K. Murase, T. Mochida, H. Sugama, Experimental and numerical studies on liquid bridge formed among three spheres, Granul. Matter 6 (2004) 111–119, http://dx.doi.org/10.1007/s10035-004-0168-8.
[35] K. Murase, T. Mochida, Y. Sagawa, H. Sugama, Estimation on the strength of a liquid bridge adhered to three spheres, Adv. Powder Technol. 19 (2008) 349–367, http://dx.doi.org/10.1163/156855208X314949.
[36] G. Gagneux, O. Millet, An analytical framework for evaluating the cohesion effects of coalescence between capillary bridges, Granul. Matter 18 (2016) 16, http://dx.doi.org/10.1007/s10035-016-0613-5.
[37] C. Semprebon, M. Scheel, S. Herminghaus, R. Seemann, M. Brinkmann, Liquid morphologies and capillary forces between three spherical beads, Phys. Rev. E 94 (2016) http://dx.doi.org/10.1103/PhysRevE.94.012907.
[38] K. Brakke, The surface evolver and the stability of liquid surfaces, Philos. Trans. R. Soc. Lond. A Math. Phys. Eng. Sci. 354 (1996) 2143–2157.
[39] Z. Fournier, D. Geromichalos, S. Herminghaus, M.M. Kohonen, F. Mugele, M. Scheel, M. Schulz, B. Schulz, C. Schier, R. Seemann, A. Skudelny, Mechanical properties of wet granular materials, J. Phys. Condens. Matter 17 (2005) S477–S502, http://dx.doi.org/10.1088/0953-8984/17/9/013.
[40] P. Pierrat, H.S. Caram, Tensile strength of wet granular materials, Powder Technol. 91 (1997) 83–93.
[41] N. Lu, B. Wu, C. Tan, Tensile strength characteristics of unsaturated sands, J. Geotech. Geoenviron. Eng. 133 (2007) 144–154.
[42] E.E. Alonso, A. Gens, A. Josa, A constitutive model for partially saturated soils, Géotechnique 40 (1990) 405–430, http://dx.doi.org/10.1680/geot.1990.40.3.405.
[43] S.J. Wheeler, V. Sivakumar, An elasto-plastic critical state framework for unsaturated soil, Géotechnique 45 (1995) 35–53, http://dx.doi.org/10.1680/geot.1995.45.1.35.
[44] M.J. Adams, S.A. Johnson, J.P.K. Seville, C.D. Willett, Mapping the influence of gravity on pendular liquid bridges between rigid spheres, Langmuir 18 (2002) 6180–6184, http://dx.doi.org/10.1021/la011823k.
[45] A. Chau, S. Régnier, A. Delchambre, P. Lambert, Theoretical and experimental study of the influence of AFM tip geometry and orientation on capillary force, J. Adhes. Sci. Technol. 24 (2010) 2499–2510, http://dx.doi.org/10.1163/016942410X508307.
[46] P. Lambert, Capillary Forces in Microassembly: Modeling, Simulation, Experiments, and Case Study, Springer, 2007.
[47] C.D. Willett, M.J. Adams, S.A. Johnson, J.P.K. Seville, Effects of wetting hysteresis on pendular liquid bridges between rigid spheres, Powder Technol. 130 (2003) 63–69, http://dx.doi.org/10.1016/S0032-5910(02)00235-8.
[48] V. Richefeu, F. Radjaï, M.S. El Youssoufi, Stress transmission in wet granular materials, Eur. Phys. J. E. Soft Matter. 21 (2006) 359–369, http://dx.doi.org/10.1140/epje/i2006-10077-1.
[49] F. Soulié, M.S. El Youssoufi, F. Cherblanc, C. Saix, Capillary cohesion and mechanical strength of polydisperse granular materials, Eur. Phys. J. E. Soft Matter. 21 (2006) 349–357, http://dx.doi.org/10.1140/epje/i2006-10076-2.
[50] T. Gröger, U. Tüzün, D.M. Heyes, Modelling and measuring of cohesion in wet granular materials, Powder Technol. 133 (2003) 203–215, http://dx.doi.org/10.1016/S0032-5910(03)00093-7.
[51] U. El Shamy, T. Gröger, Micromechanical aspects of the shear strength of wet granular soils, Int. J. Numer. Anal. Methods Geomech. 32 (2008) 1763–1790, http://dx.doi.org/10.1002/nag.695.